An oxygen barometer for rutile-ilmenite assemblages: Oxidation state of metasomatic agents in the mantle

Article *in* Earth and Planetary Science Letters · March 1999

DOI: 10.1016/S0012-821X(98)00281-7

CITATIONS
50

READS
868

3 authors, including:

Donggao Zhao
University of Missouri - Kansas City
37 PUBLICATIONS **797** CITATIONS

SEE PROFILE

Youxue Zhang
University of Michigan
140 PUBLICATIONS **6,261** CITATIONS

SEE PROFILE

ELSEVIER

Earth and Planetary Science Letters 166 (1999) 127–137

EPSL

An oxygen barometer for rutile–ilmenite assemblages: oxidation state of metasomatic agents in the mantle

Donggao Zhao [a,b], Eric J. Essene [a,*], Youxue Zhang [a]

[a] *Department of Geological Sciences, 2534 C.C. Little Building, Ann Arbor, MI 48109-1063, USA*
[b] *Department of Nuclear Engineering and Radiological Sciences, 1906 Cooley Building, Ann Arbor, MI 48109-2104, USA*

Received 30 July 1998; revised version received 21 December 1998; accepted 21 December 1998

Abstract

Oxygen fugacity has been calculated for rutile–ilmenite assemblages from the reaction $2Fe_2O_3$ (in ilmenite) + $4TiO_2$ (rutile) = $4FeTiO_3$ (in ilmenite) + O_2. The equation $\log f O_2 = 22.59 - 25925/T - 3.09 \log T + 0.0016535P + 48.836P/T - 4 \log a^{Ilm}_{FeTiO_3} + 2 \log a^{Ilm}_{Fe_2O_3} + 4 \log a^{Rut}_{TiO_2}$, where T is in kelvin and P is in kbar, was derived from available thermodynamic data. The hypothetical end-member rutile–ilmenite reaction is located between the magnetite–hematite and Ni–NiO (NNO) buffers. The rutile–ilmenite oxygen barometer has been applied to ilmenite-bearing assemblages in mantle xenoliths from kimberlites, including the metasomatic MARID (mica–amphibole–rutile–ilmenite–diopside) suite and a MORID (mica–orthopyroxene–rutile–ilmenite–diopside) vein, along with rutile–ilmenite assemblages in eclogites and in Granny Smith diopside megacrysts. The oxygen fugacities of MARID and MORID lie around the NNO buffer and are comparable to those in metasomatized spinel lherzolites. Most MARID and MORID assemblages yield a more oxidizing $f O_2$ than the EMOD (enstatite–magnesite–olivine–diamond) buffer, such that MARID and MORID fluid or melt would tend to destroy diamond or graphite by oxidation.

Keywords: rutile; ilmenite; oxygen; mantle; xenoliths; kimberlite; diamond; metasomatic rocks

1. Introduction

The oxidation state of the mantle provides a fundamental constraint on mantle processes. Several methods have been developed to calculate oxygen fugacity ($f O_2$) in various mantle assemblages [1–9]. The most widely used oxygen barometer for mantle rocks applies the reaction $6FeSiO_3$ (in orthopyroxene) + $2Fe_3O_4$ (in spinel) = $6Fe_2SiO_4$ (in olivine) + O_2 [4–8]. For example, Wood et al. [7] used this method on peridotite xenoliths from continental localities to obtain oxygen fugacities near those of the fayalite–magnetite–quartz (FMQ) buffer. The equilibrium $2Fe_2O_3$ (in ilmenite) + $4FeSiO_3$ (in orthopyroxene) = $4Fe_2SiO_4$ (in olivine) + O_2 has been applied to megacrysts, mineral intergrowths, and peridotites from kimberlites and minettes [1]. The resultant values of $\log f O_2$ derived from the various equilibria fall mostly between FMQ −1.5 and FMQ +1.5 [7], with mid-oceanic ridge basaltic glasses and unmetasomatized mantle rocks below FMQ [7,8,11]. Esseneite and acmite components in clinopyroxene coexisting with olivine and orthopyroxene have also been used to characterize oxygen fugacity in mantle assemblage [9]. In addition, oxygen fugacities

* Corresponding author. Tel.: +1-734-764-8243; Fax: +1-734-763-4690; E-mail: essene@umich.edu

0012-821X/99/$ – see front matter
PII: S0012-821X(98)00281-7

of mantle rocks have been measured by the intrinsic fO_2 method [3], although this method may not record fO_2 conditions of the xenolith at the time of equilibration in the mantle [7,10].

The redox state of mantle metasomatism has been characterized by applying orthopyroxene–spinel–olivine oxygen barometer to metasomatized spinel-bearing peridotite xenoliths [5,8,11]. It was found that mantle metasomatism recorded by peridotites from continental basalts appears to be coupled with oxidation, i.e., oxidation state increases with increasing degree of metasomatism [8], and that metasomatizing agents are more oxidizing than primitive mantle [12]. Extensively metasomatized mantle xenoliths with phlogopite, K-richterite and Ti- and Mn-enriched chromite yield fO_2 about 1.5 log unit above FMQ [8]. Mantle xenoliths brought up by kimberlites include MARID (mica–amphibole–rutile–ilmenite–diopside) suites, which are believed to form by mantle metasomatism [13,14] or from melts [15]. Waters [16] systematically studied about 50 MARID and related suites from the Bultfontein, De Beers, Wesselton, Dutoitspan and Newlands kimberlite pipes in southern Africa. Therefore, the oxidation state of the MARID suite may provide additional information about mantle metasomatism (e.g., [17]). The oxidation state of the MARID suite has not yet been studied systematically, and both oxidizing [13] and reducing [18] conditions have been suggested based on qualitative arguments such as high Fe^{3+} in diopside and low Fe^{3+}/Fe^{2+} ratio in ilmenite. We have described a metasomatic assemblage containing phlogopite–orthopyroxene–rutile–ilmenite–diopside–chromite (referred to as MORID hereafter) in a garnet–spinel lherzolite xenolith [1] in the Nikos kimberlites, Somerset Island, Northwest Territories, Canada [19]. MORID-type assemblages were previously reported in [13,16]. Given a similar enrichment in H, K, Ti and Fe, the MORID assemblage probably has a related metasomatic or melt origin as the MARID suite. Motivated by an attempt to constrain chemical conditions of mantle metasomatism in the MARID and MORID suites, we describe here an oxygen barometer using rutile and ilmenite, which are two characteristic phases in these suites.

Carmichael and Nicholls [36] suggested that ilmenite coexisting with rutile in eclogite could be used to estimate fO_2 using the reaction (referred to as RI hereafter) [2]:

$$2\,Fe_2O_3\ (\text{in ilm}) + 4\,TiO_2\ (\text{rut}) = 4\,FeTiO_3\ (\text{in ilm}) + O_2 \quad (1)$$

Two comments may clarify the use of this reaction: (i) although only ilmenite solid solution that is low in Fe^{3+} can coexist with rutile at low pressures owing to the formation of pseudobrookite solid solution, at high pressures and/or low to moderate temperatures, pseudobrookite group minerals (including armalcolite) are unstable and hence the above assemblage can serve as an oxygen barometer [37,38]; (ii) the single phase ilmenite by itself does not fix oxygen fugacity but only limits oxygen fugacity. Woermann et al. [39] contoured fO_2 isobars for Fe_2O_3–$FeTiO_3$–$MgTiO_3$ solid solution in equilibrium with an undesignated spinel; their result was erroneously applied by later workers in the absence of spinel (e.g., some applications in Haggerty [17] were for ilmenite ± spinel).

Grambling [40] used the Gibbs method to estimate $\Delta\mu O_2$ (and hence $\Delta \log fO_2$) at 4 kbar for coexisting rutile and ilmenite in crustal rocks with this reaction by assuming an ideal model for ilmenite solid solution. He obtained fO_2 for a reference sample with coexisting hematite and ilmenite phases [41] and then calculated fO_2 for other samples with coexisting rutile and ilmenite by using the reference fO_2 and the estimated $\Delta \log fO_2$. His model cannot be applied if a reference fO_2 is not available and in any case mixing of Fe_2O_3–$FeTiO_3$–$MgTiO_3$ in ilmenite is not ideal [42,43]. In this paper, we formulate the rutile–ilmenite oxygen barometer using available thermodynamic data and non-ideal mix-

[1] The transition between garnet lherzolite and spinel lherzolite in the system MAS is represented by the univariant reaction $2Mg_2Si_2O_6 + MgAl_2O_4 = Mg_3Al_2Si_3O_{12} + Mg_2SiO_4$, and the addition of Cr_2O_3 to the system changes the univariant boundary to a wide divariant field extending the stability of spinel–enstatite to much higher pressure [20]. Therefore, garnet–chromite lherzolite is an expected divariant assemblage and is not uncommon in kimberlites [21–35].

[2] This oxygen barometer can be combined with the two-oxide barometer to produce the following oxygen barometer: $2Fe_3O_4$ (in chromite) + $3TiO_2$ (rutile) = $3Fe_2TiO_4$ (in chromite) + O_2.

ing models for rhombohedral oxides in the system Fe_2O_3–$FeTiO_3$–$MgTiO_3$.

2. Formulation of the oxygen barometer

The oxygen fugacities of assemblages containing both rutile and ilmenite can be calculated from the equilibrium constant of reaction (1). At equilibrium,

$$2.303RT\log\left(\frac{(fO_2)(a^{Ilm}_{FeTiO_3})^4}{(a^{Ilm}_{Fe_2O_3})^2(a^{Rut}_{TiO_2})^4}\right) = -\Delta G^P_T$$

$$= -\left(\Delta G^0_T + \int_1^P \Delta V_s \mathrm{d}P\right) \quad (2)$$

where R is the gas constant in J mol^{-1} K^{-1}, T is in kelvin, P in bar, ΔG^P_T and ΔG^0_T are the Gibbs free energy (J) of the end-member reaction at (T, P) and at (T, 1 bar), and ΔV_s is the volume difference between the solid product and reactants in J/bar. In evaluating ΔG and ΔV_s, Fe_2O_3 in hematite is used as the standard state for Fe_2O_3 in ilmenite. This approach is appropriate because the activity model for Fe_2O_3 in ilmenite also uses Fe_2O_3 in hematite as the standard state (e.g., Ghiorso [42]; Andersen et al. [43]). The ΔG^P_T for reaction (1) is evaluated from three different thermodynamic data sets [44–46]. Two data sets [45,46] yield log fO_2 nearly identical to each other (Fig. 1), while the third [44] shows small discrepancies at higher temperatures, with differences of < 0.3 log fO_2 at 1500ºC and better agreement at lower temperatures (Fig. 1). The hypothetical end-member RI reaction in log fO_2 vs. T space is located between the magnetite–hematite (MH) and the NNO buffers at 1 bar total pressure (Fig. 1). Because our calculations are related to Fe^{3+}-bearing system and because the entropy of mixing on the ilmenite–hematite and geikielite–hematite joins was explicitly formulated in Ghiorso's model [42], we select his solution model, which includes a modification of Berman's [44] standard state thermodynamic data for consistency. The ΔG^P_T was first calculated from Berman [44] (using the PerPlex program with data b92ver.dat, see Connolly [47] and http://buzzard.ethz.ch/~jamie/perplex.html) at 700–1800 K and ≤60 kbar, and then was fit to the form of $\Delta G^P_T = C_0 + C_1T + C_2T\log T + C_3P + C_4PT$, which reproduces ΔG^P_T from Berman [44] with a maximum deviation of 0.8 kJ at 700–1800 K and ≤60 kbar ($r^2 = 0.99998$), equivalent to 0.05 unit in log fO_2. Because Ghiorso [42] modified the standard state enthalpy of hematite at 298.15 K and 1 bar from Berman's −825.627 kJ/mol [44] to −822.0 kJ/mol, his modification is incorporated by subtracting 7254 J for 2 moles of hematite from the ΔG^P_T from Berman [44]. The resulting ΔG^P_T expression at 700–1800 K and ≤60 kbar is:

$$\Delta G^P_T = 496340 - 432.47T + 59.168T\log T - 934.96P - 0.031656PT \quad (3)$$

where ΔG^P_T is in J, T in kelvin and P in kbar. Substituting Eq. 3 into Eq. 2 and rearranging yield:

$$\log fO_2 = 22.59 - 25925/T - 3.09\log T + 0.0016535P + 48.836P/T - 4\log a^{Ilm}_{FeTiO_3} + 2\log a^{Ilm}_{Fe_2O_3} + 4\log a^{Rut}_{TiO_2} \quad (4)$$

Therefore, oxygen fugacities of assemblages containing both rutile and ilmenite may be calculated from the activities of $FeTiO_3$, Fe_2O_3 and TiO_2 by Eq. 4 at a given P and T. If rutile is not present, the RI oxygen barometer can be applied to single ilmenite crystals to obtain an upper limit of fO_2. Because the ΔV_s values for NNO and RI reactions are similar (−0.876 J/bar for NNO and −0.902 J/bar for RI at 1 bar and 298.15 K), the pressure effect nearly cancels if log fO_2 from the RI oxygen barometer is normalized to log fO_2 from the NNO buffer. The major component in rutile is TiO_2 (usually >95 wt%); the mole fraction of TiO_2 in rutile is used as the activity of TiO_2.

3. Sources of error

One source of uncertainty is from the mixing model [42,43] used to calculate the activities of Fe_2O_3 and $FeTiO_3$ in ilmenite, especially the uncertainty associated with the dependence of activity model on pressure, which has not yet been accounted for by available mixing models. Furthermore, the two mixing models for the ilmenite solid solution [42,43] do not result in similar activities. To compare results from the two models, log fO_2 values are calculated by (i) using Eq. 4 with activities from

Table 1
Oxygen fugacities of various assemblages calculated from rutile–ilmenite (RI) and other oxygen barometers

Sample No.	T [a] (K)	P [a] (kbar)	Mole fractions						Activities			log fO_2	Δ log fO_2	log fO_2	log fO_2
			$MgTiO_3$	Fe_2O_3	$FeTiO_3$	$MnTiO_3$	TiO_2 (Rut)	$Fe^{3+}/\sum Fe$	Fe_2O_3	$FeTiO_3$	TiO_2	RI [b]	RI [b]–NNO [c]	Sp–Ilm [d]	Ol–Opx–Sp [e]
MARID															
1158	1300	36	0.386	0.058	0.547	0.009	0.923	0.176	0.021	0.629	0.923	−8.3	0.3		
AJE288	1300	36	0.367	0.045	0.577	0.012	0.820	0.136	0.013	0.659	0.820	−8.9	−0.3		
AJE326-1	1300	36	0.452	0.093	0.451	0.004	0.946	0.291	0.045	0.534	0.946	−7.3	1.3		
AJE326-3/1	1300	36	0.542	0.027	0.425	0.006	0.946	0.114	0.006	0.553	0.946	−9.1	−0.5		
BF18-1	1300	36	0.448	0.048	0.497	0.007	0.972	0.162	0.015	0.601	0.972	−8.3	0.2		
JJG2315-1	1300	36	0.324	0.055	0.613	0.008	0.898	0.153	0.019	0.675	0.898	−8.5	0.1		
JJG2316-1	1300	36	0.252	0.066	0.673	0.009	0.893	0.164	0.024	0.702	0.893	−8.4	0.2		
JJG2316-4/1	1300	36	0.396	0.080	0.516	0.009	0.893	0.237	0.035	0.590	0.893	−7.8	0.8		
JJG2328	1300	36	0.322	0.050	0.622	0.006	0.961	0.139	0.016	0.687	0.961	−8.6	0.0		
AJE214 [f]	1300	36	0.353	0.075	0.566	0.006	0.960	0.210	0.031	0.629	0.960	$\leq$−7.8	0.8		
AJE281 [f]	1300	36	0.339	0.075	0.580	0.007	0.960	0.205	0.031	0.638	0.960	$\leq$−7.9	0.7		
AJE294 [f]	1300	36	0.300	0.056	0.633	0.011	0.960	0.150	0.018	0.686	0.960	$\leq$−8.4	0.1		
AJE31 [f]	1300	36	0.387	0.075	0.530	0.007	0.960	0.221	0.032	0.604	0.960	$\leq$−7.8	0.8		
AJE333 [f]	1300	36	0.399	0.064	0.529	0.007	0.960	0.195	0.025	0.612	0.960	$\leq$−8.0	0.6		
AJE66 [f]	1300	36	0.303	0.080	0.607	0.010	0.960	0.208	0.033	0.650	0.960	$\leq$−7.8	0.7		
FW12 [f]	1300	36	0.459	0.037	0.498	0.006	0.960	0.131	0.010	0.610	0.960	$\leq$−8.8	−0.2		
FW26A [f]	1300	36	0.486	0.029	0.479	0.005	0.960	0.109	0.007	0.601	0.960	$\leq$−9.1	−0.5		
JJG2319 [f]	1300	36	0.381	0.075	0.535	0.009	0.960	0.219	0.031	0.607	0.960	$\leq$−7.8	0.8		
JJG2331 [f]	1300	36	0.308	0.050	0.630	0.012	0.960	0.137	0.015	0.689	0.960	$\leq$−8.6	0.0		
JJG2332 [f]	1300	36	0.302	0.061	0.624	0.013	0.960	0.165	0.022	0.675	0.960	$\leq$−8.3	0.3		
Other															
JP1-X17 (MORID vein)	1300	36	0.480	0.062	0.454	0.004	0.952	0.215	0.024	0.556	0.952	−7.9 ± 0.7	0.7	−8.0	
JP1-X17 (lherzolite host)	1300	36													−7.9
BD2394 (Rut–Ilm–Sp vein)	1500	50	0.539	0.042	0.415	0.004	0.908	0.167	0.008	0.534	0.908	−6.0	−0.2	−5.9	
PHN2793/8B (eclogite)	1300	36	0.504	0.049	0.442	0.005	0.962	0.182	0.017	0.553	0.962	−8.2	0.4		
A-306 (eclogite)	1300	36	0.396	0.040	0.561	0.003	0.970	0.125	0.011	0.657	0.970	−8.8	−0.2		
BD2997A (Granny Smith diopside)	1300	36	0.494	0.040	0.462	0.004	0.910	0.146	0.011	0.578	0.910	−8.7	−0.1		

[a] P and T estimated from the host assemblage of JP1-X17 are used for samples except for BD2394 [54], which is from a diamond mine and the minimum pressure for diamond to be stable at 1500 K [55] is used. The pressure effect is negligible when log fO_2 is expressed relative to NNO.
[b] This study, Ghiorso's solution model and Ghiorso modified Berman thermodynamic data used [42,44]. Uncertainty is given for the MORID vein only because the other data are from literature without specified uncertainties.
[c] NNO from [8].
[d] Thermodynamic data from [42,44], solution models from [42,53].
[e] Using [7].
[f] $X(TiO_2)$ assumed to be 0.96. Sample sources: MARID samples from [16], table 12.1, except for 1158, which is from [13] (ilmenite is the average of 1 and 2 in table 5, rutile has 2–5 wt% Nb_2O_5). AJE214 and 288 are MARI (missing Cpx). JP1-X17 from [19]. BD2394 from [54], coexisting ilmenite, rutile and chromite in the vein in polymict xenolith, from the Bultfontein diamond mine. PHN2793/8B from [56]. A-306 from [57], ilmenite in rutile. BD2997A from [58], rutile and ilmenite intergrowth inside Granny Smith diopside megacryst.

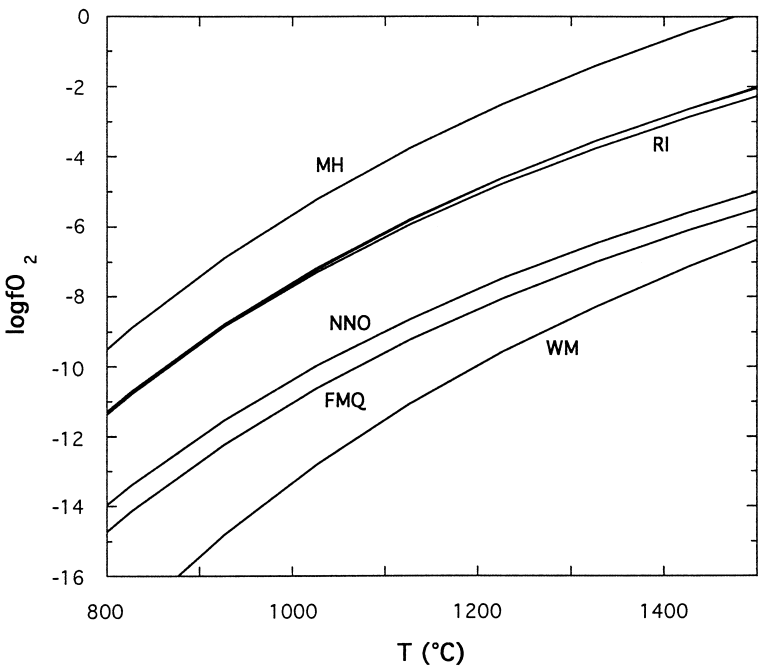

Fig. 1. log fO_2 vs. T for several oxygen buffer reactions at 1 bar. *MH* = magnetite–hematite; *RI* = rutile–ilmenite; *NNO* = Ni–NiO; *FMQ* = quartz–fayalite–magnetite; *WM* = wüstite($Fe_{0.947}O$)–magnetite. The RI buffer curves are calculated using data from [44–46] for comparison. The thick curve of RI is from [45] and [46]; the thin curve immediately below is from [44] with modification from Ghiorso [42]. Other buffer curves are calculated using data from [46] only.

the model of Ghiorso [42], and (ii) using ΔG_T^P for reaction (1) from the thermodynamic data of Robie et al. [48] (use of this data base is necessary to maintain self-consistency), volume data of Berman [44], and the mixing model of Andersen et al. [43]. For ilmenite containing $X(MgTiO_3)$ of 0.4–0.5 and $X(Fe_2O_3)$ of 0.05–0.1, the difference between the calculated log fO_2 from the two mixing models is $<$1.0 log unit. Another T–X region where the two models agree within 1 log unit is at $\sim$900 K and with $X(FeTiO_3)$ of 0.3 to 0.8. However, outside the T–X regions, the log fO_2 differences between the two models become larger, e.g., up to 5 log units for ilmenite with $X(FeTiO_3) = 0.01$, $X(MgTiO_3) = 0.60$ and $X(Fe_2O_3) = 0.39$ at 627ºC and 5 kbar, with the model of Andersen et al. [43] usually giving more oxidizing results. When the RI oxygen barometer is applied to Grambling's ilmenite–rutile–hematite assemblage at 500ºC and 4 kbar [40], the model of Ghiorso [42] yields log fO_2 of -19.1 and -19.9 for the hematite solid solution–rutile pair and for the ilmenite solid solution–rutile pair, respectively. These two values are close to each other and also close to an independent estimate (log fO_2 of -20) from hematite–ilmenite [41]. In contrast, the model of Anderson et al. [43] results in log fO_2 of -20.9 for the hematite solid solution–rutile pair and -18.1 for the ilmenite solid solution–rutile pair. The mixing model from Ghiorso [42] is provisionally adopted in this paper. However, because of the discrepancies between the two solution models for ilmenite, caution should be exercised if the RI oxygen barometer is applied to crustal assemblages. For the applications discussed below in this paper (Table 1), the composition of ilmenite is such that the two mixing models give fO_2 within 1 log unit.

A second source of uncertainty associated with the RI oxygen barometer arises from calculating $X(Fe_2O_3)$ from electron microprobe analyses (EMPA) of ilmenite by stoichiometry and charge balance. We evaluated both the precision and accuracy as follows.

(1) The precision is obtained from repeated microprobe analysis of ilmenite in a sample. For ex-

ample, the average composition of 11 analyses of an ilmenite grain in the MORID vein (JP1-X17) in wt% is SiO_2 0.03 ± 0.03 (2σ uncertainty hereafter), TiO_2 55.51 ± 1.11, Al_2O_3 0.29 ± 0.40, Cr_2O_3 0.69 ± 0.35, V_2O_3 0.13 ± 0.09 (corrected for Ti interference [49]), TFeO 27.97 ± 1.82, MnO 0.26 ± 0.05, MgO 14.45 ± 0.68, ZnO 0.02 ± 0.08. Because FeO and MgO co-vary negatively, only part of the compositional variations is due to counting error and the other part is due to real heterogeneity of the sample. Calculated $X(Fe_2O_3)$ and $\log fO_2$ for the 11 analyses are 0.04 ± 0.02 (2σ uncertainty hereafter) and -8.8 ± 0.7 (at 1300 K and 36 kbar), respectively. The 2σ uncertainties on the mean of calculated $X(Fe_2O_3)$ and $\log fO_2$ are 0.006 and 0.2. As the $X(Fe_2O_3)$ in ilmenite increases or decreases, the relative uncertainty in $X(Fe_2O_3)$ and hence in calculated $\log fO_2$ decreases or increases if the absolute error in $X(Fe_2O_3)$ stays the same.

(2) Another critical issue for calculated $X(Fe_2O_3)$ from EMPA is its accuracy (e.g., [8,10,50]). That has been assessed by comparing results from EMPA with those from Mössbauer measurements. Virgo et al. [10] compared EMPA and Mössbauer results and concluded that apparently precise EMPA results are not necessarily an indication of a high level of accuracy. The EMPA correction procedures and the choice of different standards may affect the calculated $Fe^{3+}/(Fe^{3+} + Fe^{2+})$ ratios [10]. To increase accuracy in calculating $X(Fe_2O_3)$, an EMP procedure must analyze all major elements accurately (high precision is not enough) and must also include all minor elements. Hence, the accuracy of the calculated $X(Fe_2O_3)$ is expected to depend on accuracy and homogeneity of standards, whether necessary minor elements are analyzed, and experience of the operator. Some ilmenite samples, for which Mössbauer measurements of $Fe^{3+}/(Fe^{3+} + Fe^{2+})$ were obtained by Virgo et al. [10], were analyzed on the University of Michigan electron microprobe using regular analytical procedure for magnesian ilmenite, which was designed before obtaining samples from Virgo. The standards used are $MgTiO_3$ (synthetic) for Mg, ilmenite for Ti and Fe, $MgAl_2O_4$ (synthetic) for Al, V_2O_5 (synthetic) for V, clinopyroxene (PX69) for Si, $Ca_3Cr_2Si_3O_{12}$ (synthetic) for Cr, rhodonite (Broken Hill) for Mn, and ZnS (synthetic) for Zn. The ilmenites were analyzed at an accelerating voltage of 15 kV and a beam current of 10 nA. The V_2O_3 content was corrected for Ti K_β interference by subtracting 0.0042 wt% TiO_2 from the original value for V_2O_3. The coefficient 0.0042 was obtained by analyzing the synthetic TiO_2 and $MgTiO_3$ for apparent V. The calculated $Fe^{3+}/(Fe^{3+} + Fe^{2+})$ ratios for these samples analyzed at the University of Michigan, as well as those analyzed at other institutes, are compared with Mössbauer determinations (Fig. 2). The agreement between our calculated $Fe^{3+}/(Fe^{3+} + Fe^{2+})$ ratios (as well as those from microprobe analyses at Pennsylvania State University) and Mössbauer determinations is very good (Fig. 2). We conclude that our electron microprobe analyses of ilmenite are of high enough quality for accurate calculation of the $Fe^{3+}/(Fe^{3+} + Fe^{2+})$ ratios.

The estimation of a minor ferric component from EMPA is a problem shared by all currently used oxygen barometers applied to mantle assemblages. For example, use of the oxygen barometers for olivine–orthopyroxene–spinel, olivine–orthopyroxene–ilmenite, and ilmenite–spinel requires estimation of minor Fe_3O_4 in spinel, Fe_2O_3 in ilmenite, or both. We have demonstrated above that at least for ilmenite, careful electron microprobe analyses yield $Fe^{3+}/(Fe^{3+} + Fe^{2+})$ similar to those from Mössbauer analyses, albeit with larger relative errors (Fig. 2). Ballhaus et al. [8] have also argued that reservations on the calculation of Fe_3O_4 component in spinel from microprobe analyses are unfounded (see also [51]).

Summarizing the above results, our assessment of the RI oxygen barometer is as follows.

(1) The standard state properties are well known for the purpose of oxygen barometry in mantle assemblages.

(2) Careful electron microprobe analyses can be used to obtain reliable $X(Fe_2O_3)$. Estimating $X(Fe_2O_3)$ from EMPA of Fe_2O_3-poor ilmenite yields relatively large uncertainties in the oxygen barometer, but the uncertainty is reduced for ilmenite containing high Fe_2O_3.

(3) The main source of uncertainties is from the mixing models of ilmenite. Improvement of the model will be important to this oxygen barometer. At present, the barometer is best applied to assemblages with ilmenite which has $X(FeTiO_3)$ close to or more than $X(MgTiO_3)$, or $X(Fe_2O_3)$ around 0.1 or 0.7.

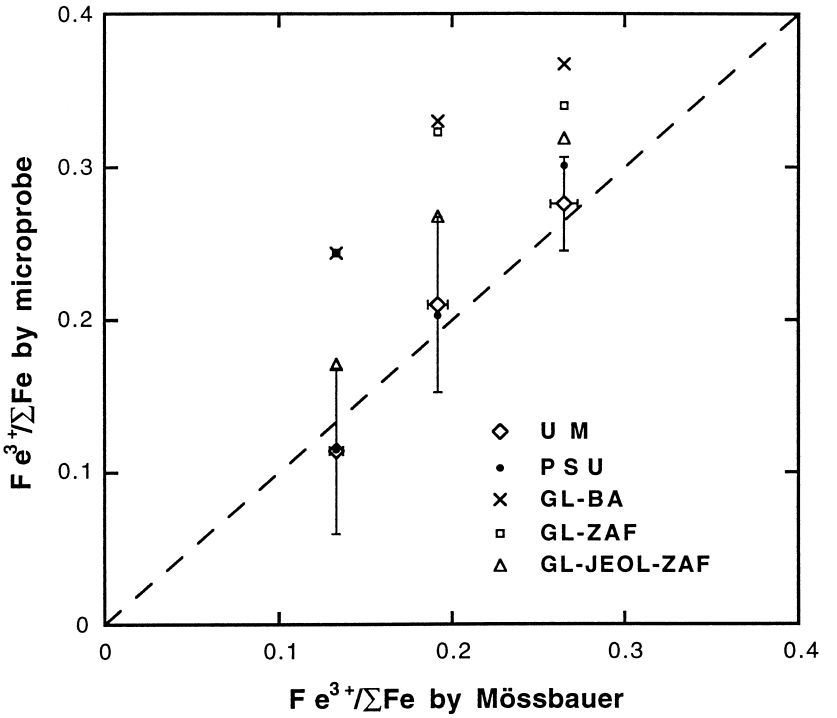

Fig. 2. Comparison of calculated $Fe^{3+}/(Fe^{3+} + Fe^{2+})$ ratios using microprobe analyses from various laboratories (vertical axis) with the Mössbauer measurements of Virgo et al. [10]. Three samples (ULM 2, Yakutia-Dalnaya No. 1 D-46/79, and ROM 264 IL-41) used in the comparison were provided by D. Virgo. Legend: *U M* = University of Michigan, ZAF correction; *P S U* = Pennsylvania State University, Bence-Albee correction; *GL-BA* = Geophysical Lab, Bence-Albee correction; *GL-ZAF* = Geophysical Lab, ZAF correction; *GL-JEOL-ZAF* = Geophysical Lab, JEOL-SEM, ZAF correction. Results of UM microprobe analyses are from this work. Results of other microprobe analyses are from Virgo et al. [10]. The solid line is a 1:1 line. Shown are also 2σ error bars for Mössbauer analyses (3% relative, D. Virgo, pers. commun.) and for repeated microprobe analyses at the University of Michigan.

With the above precautions, the RI oxygen barometer provides a method to characterize redox state of assemblages containing both rutile and ilmenite.

4. Comparison with other oxygen barometers

Comparisons with other oxygen barometers confirm that the RI oxygen barometer for the P–T–X under consideration is accurate to less than 1 log fO_2 unit. The MORID vein in sample JP1-X17 [19] contains rutile, ilmenite, and spinel. The log fO_2 calculated from the RI barometer (−7.9) agrees well with that calculated from the spinel–ilmenite oxygen barometer (−8.0) (Table 1). The log fO_2 of the host lherzolite (JP1-X17) calculated using olivine–orthopyroxene–spinel oxygen barometer (−7.9) is similar to that in the MORID vein.

A vein in a polymict xenolith (BD2394) from the Bultfontein diamond mine, South Africa contains coexisting ilmenite, chromite and rutile [54]. At 50 kbar, the minimum pressure for diamond to be stable at 1500 K [55], the fO_2 calculated from RI (−6.0) is in excellent agreement with that from spinel–ilmenite (−5.9) (Table 1).

5. Applications

The RI oxygen barometer may be applied to coexisting rutile–ilmenite in MORID vein [19], MARID suites [13,16], eclogitic xenoliths from kimberlite [56,57] and an assemblage from a 'Granny Smith' diopside megacryst [58] (Table 1; Fig. 3). For the MORID vein, T and P are estimated to be 1300 K and 36 kbar from two-pyroxene thermometry

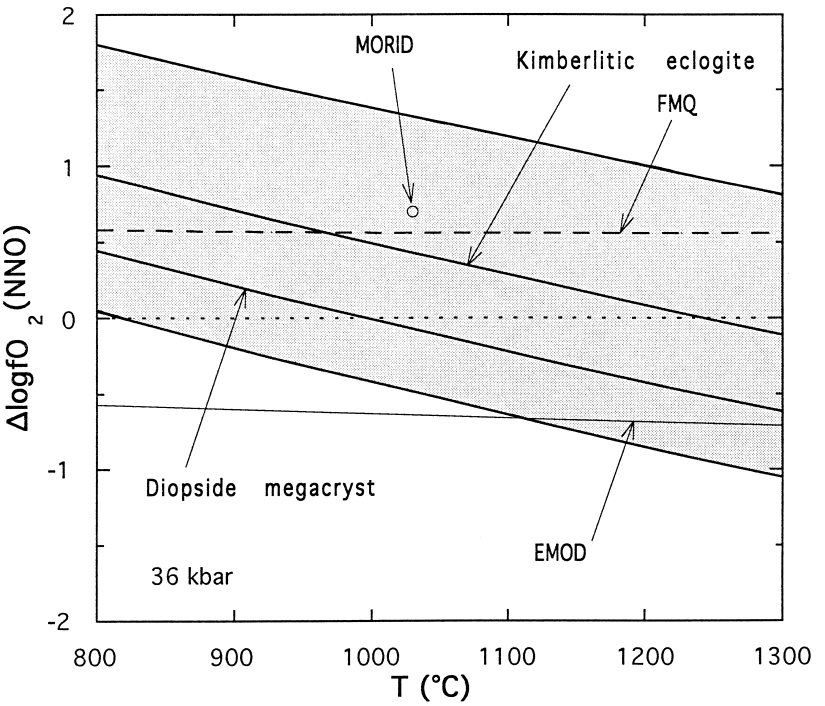

Fig. 3. log fO_2 (normalized to NNO) vs. T obtained from the RI oxygen barometer for different rutile–ilmenite assemblages. Only for MORID vein [19] can a unique value of fO_2 be obtained (circle). The range of fO_2 (shaded area) obtained from MARID assemblages in the literature [13,16] is approximately 1 log unit below to 2 log units above NNO. Ilmenite–rutile from a kimberlitic eclogite [56] and ilmenite–rutile in a 'Granny Smith' diopside megacryst [58] show similar fO_2 to MARID suites. For comparative purposes, 36 kbar, which is estimated from the host assemblage (JP1-X17) of MORID, was used for all samples in the diagram when calculating fO_2. The assumption of 36 kbar for MARID assemblages is consistent with experiments [14,15,52]. Use of a $\Delta \log fO_2$ minimizes any variation with pressure. NNO is from [8]. FMQ and EMOD are calculated from thermodynamic data [45].

[59] and orthopyroxene–garnet barometry [59] in the host lherzolite. For MARID suites and other rutile–ilmenite assemblages, no $T-P$ estimates are available. Since the pressure effect on the RI buffer is similar to that on NNO buffer, log fO_2 relative to NNO is roughly independent of pressure and an arbitrary pressure of 36 kbar is chosen for MARID suites. The uncertainty in T introduces considerable uncertainty in log fO_2 (Fig. 3). In order to constrain the fO_2, it is necessary in future work to constrain the equilibrium T for the rutile–ilmenite equilibrium. Without such constraints, we simply use an arbitrary lower temperature limit of 800°C and an upper temperature limit of 1300°C (the solidus of MARID without excess H_2O is 1260°C at 30 kbar [52]).

The fO_2 inferred from MORID vein is slightly more oxidizing than the FMQ buffer ($\Delta \log fO_2$ (FMQ) = 0.17), more oxidizing than unmetasomatized peridotite xenoliths, and comparable to fO_2 of metasomatized spinel peridotites [8,11]. The fO_2 inferred from MARID suites covers two log units at any given T and covers that of MORID, kimberlitic eclogite, and a 'Granny Smith' diopside megacryst. Although the large uncertainty in T for MARID assemblages does not allow simple comparisons to be made, the log fO_2 values of MARID suites (Fig. 3) are generally consistent with metasomatized peridotites [8,11]. Even with allowance of large temperature uncertainty, 17 out of 20 MARID samples have fO_2 more oxidizing than EMOD (Fig. 3; Table 1). Hence our data on MORID vein and MARID suites support the conclusion that metasomatizing agents are typically more oxidizing than unmetasomatized mantle [8,11].

The oxygen fugacity of the upper mantle strongly

influences the stability of diamond/graphite, fluids and carbonates. Under reducing conditions, diamond or graphite is stable, while under oxidizing conditions CO_2 or carbonates are stable. The fO_2 for diamond in olivine-bearing assemblages must be less than that defined by the enstatite–magnesite–olivine–diamond/graphite (EMOD/EMOG) equilibrium [60]:

$$MgSiO_3 \text{ (enstatite)} + MgCO_3 \text{ (magnesite)} = Mg_2SiO_4 \text{ (olivine)} + C \text{ (diamond/graphite)} + O_2 \quad (5)$$

The shift of the above oxygen buffer owing to solid solutions in the minerals is very small in ultramafic rocks. Experimental calibrations of the EMOD buffer published in two abstracts [60,61] show differences of 0.6 log fO_2 at 1400 K and 50 kbar. Calculation of EMOD from thermodynamic data [45,46,62] gives values between the two experimental calibrations. The EMOD buffer calculated from Holland and Powell [45] ($\log fO_2 = 15.28 - 25775/T - 2.08767 \log T + 0.0026P + 62P/T$ where T is in K and P is in kbar) is selected to compare with the fO_2 obtained from the RI oxygen barometer to evaluate the diamond potential of the Nikos kimberlites, Somerset Island, Northwest Territories, Canada. The MORID vein in the garnet–spinel lherzolite xenolith (JP1-X17) and most MARID assemblages (Fig. 3) yield a more oxidizing fO_2 than EMOD; thus, the MORID and MARID fluid or melt would tend to destroy existing diamond or graphite by oxidation, and magnesite should be favored over carbon polymorphs in these olivine-bearing assemblages.

Acknowledgements

This research was supported by a research fund from the Government of Canada to EJE, C.M. Hall and YZ, EAR-9706107 and 9458368 to YZ, EAR-9117772 and 9526596 to EJE, the Scott Turner Award of the University of Michigan to DZ, and a research grant of Geological Society of America to DZ. We thank A.J. Pell for providing xenolith samples and F. Waters for providing analytical data on the MARID assemblages from her Ph.D. thesis. We are especially grateful to David Virgo for the loan of ilmenite samples. This paper benefited from discussions with Liping Wang. M.S. Ghiorso, R.W. Luth, S.E. Haggerty and an anonymous reviewer are thanked for their comments. ***[RV]***

References

[1] D.H. Eggler, Upper mantle oxidation state: evidence from olivine–orthopyroxene–ilmenite assemblages, Geophys. Res. Lett. 10 (1983) 365–368.
[2] S.E. Haggerty, L.A. Tompkins, Subsolidus reactions in kimberlitic ilmenite: exsolution, reduction and the redox state of the mantle, in: J. Kornprobst (Ed.), Kimberlites I: Kimberlites and Related Rocks, Proc. 3rd Int. Kimb. Conf., Elsevier, Amsterdam, 1984, pp. 335–357.
[3] R.J. Arculus, Oxidation status of the mantle: past and present, Annu. Rev. Earth Planet. Sci. 13 (1985) 75–95.
[4] H.S.C. O'Neill, V.J. Wall, The olivine–orthopyroxene–spinel oxygen geobarometer, the nickel precipitation curve, and the oxygen fugacity of the Earth's upper mantle, J. Petrol. 28 (1987) 1169–1191.
[5] G.S. Mattioli, M.B. Baker, M.J. Rutter, E.M. Stolper, Upper mantle oxygen fugacity and its relationship to metasomatism, J. Geol. 97 (1989) 521–536.
[6] L.T. Bryndzia, B.J. Wood, Oxygen thermobarometry of abyssal spinel peridotites: the redox state and C–O–H volatile composition of the Earth's sub-oceanic upper mantle, Am. J. Sci. 290 (1990) 1093–1116.
[7] B.J. Wood, L.T. Bryndzia, K.E. Johnson, Mantle oxidation state and its relationship to tectonic environment and fluid speciation, Science 248 (1990) 337–345.
[8] C.G. Ballhaus, R.F. Berry, D.H. Green, High pressure experimental calibration of the olivine–orthopyroxene–spinel oxygen geobarometer: implications for the oxidation state of the upper mantle, Contrib. Mineral. Petrol. 107 (1991) 27–40.
[9] R.W. Luth, D. Canil, Ferric iron in mantle-derived pyroxenes and a new oxybarometer for the mantle, Contrib. Mineral. Petrol. 113 (1993) 236–248.
[10] D. Virgo, R.W. Luth, M.A. Moats, G.C. Ulmer, Constraints on the oxidation state of the mantle: an electrochemical and ^{57}Fe Mössbauer study of mantle-derived ilmenites, Geochim. Cosmochim. Acta 52 (1977) 1781–1794.
[11] C. Ballhaus, Redox states of lithospheric and asthenospheric upper mantle, Contrib. Mineral. Petrol. 114 (1993) 331–348.
[12] D.H. Green, M.E. Wallace, Mantle metasomatism by ephemeral carbonatite melts, Nature 336 (1988) 459–462.
[13] J.B. Dawson, J.V. Smith, The MARID (mica–amphibole–rutile–ilmenite–diopside) suite of xenoliths in kimberlite, Geochim. Cosmochim. Acta 41 (1977) 309–323.
[14] R.J. Sweeney, A.B. Thompson, P. Ulmer, Phase relations of a natural MARID composition and implications for MARID genesis, lithospheric melting and mantle metasomatism, Contrib. Mineral. Petrol. 115 (1993) 225–241.
[15] F.G. Waters, A suggested origin of MARID xenoliths in

kimberlites by high pressure crystallization of an ultrapotassic rock such as lamproite, Contrib. Mineral. Petrol. 95 (1987) 523–533.
[16] F.G. Waters, A Geochemical Study of Metasomatised Peridotite and MARID Nodules from the Kimberley Pipes, South Africa, PhD thesis, University of Cape Town, 1987.
[17] S.E. Haggerty, Upper mantle opaque mineral stratigraphy and the genesis of metasomites and alkali-rich melts, in: Ross et al. (Eds.), Kimberlites and Related Rocks II, Proc. 4th Int. Kimb. Conf., Blackwell, Oxford, 1989, pp. 687–699.
[18] B. Harte, J.J. Gurney, Ore mineral and phlogopite mineralization within ultramafic nodules from the Matsoku kimberlite pipe, Lesotho, Carnegie Inst. Wash. Yearb. 74 (1975) 528–536.
[19] D. Zhao, E.J. Essene, Y. Zhang, J.A. Pell, Mantle xenoliths from the Nikos kimberlites on Somerset Island and the Zulu kimberlites on Brodeur Peninsula, Baffin Island, Canada, 7th IKC Extended Abstract Volume, Cape Town, 1998, pp. 998–1000.
[20] S.A.C. Webb, B.J. Wood, Spinel–pyroxene–garnet relationships and their dependence on Cr/Al ratio, Contrib. Mineral. Petrol. 92 (1986) 471–480.
[21] A.V. Andronikov, B.V. Belyatsky, Implication of Sm–Nd isotopic systematics to the events recorded in the mantle-derived xenoliths from Jetty Peninsula, East Antarctica, Terra Antarct. 2 (1995) 103–110.
[22] A.V. Andronikov, Spinel–garnet lherzolite nodules for alkaline–ultrabasic rocks of Jetty Peninsula (East Antarctica), Antarct. Sci. 2 (1990) 321–330.
[23] I.V. Ashchepkov, Composite garnet peridotite xenolith from picrite-basalt, Vitim Plateau (Transbaikal): implication for the thermobarometry and reconstructions of the mantle sections, 5th Int. Kimb. Conf., 1991, Extended Abstracts 13.
[24] I.V. Ashchepkov, N.L. Dobretsov, M.A. Kalmanovich, Garnet peridotites, alkaline picrites and basanites from the Vitim Plateau (translated title), Dokl. Akad. Nauk SSSR 302 (1988) 417–420.
[25] F.R. Boyd, R.V. Danchin, Lherzolites, eclogites, and megacrysts from some kimberlites of Angola, Am. J. Sci. 280A (1990) 528–549.
[26] F.R. Boyd, P.H. Nixon, Ultramafic nodules from the Kimberley pipes, South Africa, Geochim. Cosmochim. Acta 42 (1985) 1367–1382.
[27] Rong-Long Cao, Shouhua Zhu, Mantle xenoliths and alkali-rich host rocks in eastern China, in: P.H. Nixon (Ed.), Mantle Xenoliths, Wiley, New York, 1987, pp. 167–180.
[28] J. Ganguly, P.K. Bhattacharya, Xenoliths in Proterozoic kimberlites from southern India: petrology and geophysical implications, in: P.H. Nixon (Ed.), Mantle Xenoliths, Wiley, New York, 1987, pp. 249–265.
[29] B.C. Hearn Jr., E.S. McGee, Garnet peridotites from Williams Kimberlite, North-Central Montana, U.S.A., in: J. Kornprobst (Ed.), Kimberlites II: Kimberlites and Related Rocks, Proc. 3rd Int. Kimb. Conf., Elsevier, Amsterdam, 1984, pp. 57–70.
[30] R.H. Mitchell, Garnet lherzolites from the hannaus-I and Louwrensia kimberlites of Namibia, Contrib. Mineral. Petrol. 86 (1984) 178–188.
[31] P.N. Nixon, F.R. Boyd, Garnet bearing lherzolites and discrete nodule suites from the Malaita alnoite, Solomon Islands, S.W. Pacific, and their bearing on oceanic mantle composition and geotherm, Proc. 2nd Int. Kimb. Conf. 2, American Geophysical Union, Washington, DC, 1979, pp. 400–423.
[32] I.D. Ryabchikov, A.V. Ukhanov, T. Ishii, Redox equilibria in upper mantle ultrabasites in the Yakutia kimberlite province, Geokhimiya 8 (1985) 1110–1122.
[33] J.V. Smith, J.B. Dawson, Chemistry of Ti-poor spinels, ilmenites and rutiles from peridotite and eclogite xenoliths, Phys. Chem. Earth 9 (1975) 309–322.
[34] N.V. Sobolev, F.V. Kaminsky, W.L. Griffin, E.S. Yefimova, T.T. Win, C.G. Ryan, A.I. Botkunov, Mineral inclusions in diamonds from the Sputnik kimberlite pipe, Yakutia, Lithos 39 (1997) 135–157.
[35] K.S. Viljoen, D.N. Robinson, P.M. Swash, W.L. Griffin, M.L. Otter, C.G. Ryan, T.T. Win, Diamond- and graphite-bearing peridotite xenoliths from the Roberts Victor kimberlite, South Africa, 5th Int. Kimb. Conf., CPRM, Spec. Publ. 1A (1994) 285–303.
[36] I.S.E. Carmichael, J. Nicholls, Iron–titanium oxides and oxygen fugacities in volcanic rocks, J. Geophys. Res. 72 (1967) 4665–4687.
[37] L.M. Anovitz, A.H. Treiman, E.J. Essene, B.S. Hemingway, E.F. Westrum Jr., V.J. Wall, R. Burriel, S.R. Bohlen, The heat-capacity of ilmenite and phase equilibria in the system Fe–Ti–O, Geochim. Cosmochim. Acta 49 (1985) 2027–2040.
[38] J.L. Hayob, E.J. Essene, Armalcolite in crustal paragneiss xenolith, central Mexico, Am. Mineral. 80 (1995) 810–822.
[39] E. Woermann, A. Hirschberg, A. Lamprecht, Das System Hämatit–Ilmenit–Geikielith unter hohen Temperaturen und hohen Drucken, Fortschr. Miner. 47 (1969) 79–80.
[40] J.A. Grambling, A regional gradient in the composition of metamorphic fluids in pelitic schist, Pecos Baldy, New Mexico, Contrib. Mineral. Petrol. 94 (1986) 149–164.
[41] K.J. Spencer, D.H. Lindsley, A solution model for coexisting iron–titanium oxides, Am. Mineral. 66 (1981) 1189–1201.
[42] M.S. Ghiorso, Thermodynamic properties of hematite–ilmenite–geikielite solid solutions, Contrib. Mineral. Petrol. 104 (1990) 645–667.
[43] D.J. Andersen, F.C. Bishop, D.H. Lindsley, Internally consistent solution models for Fe–Mg–Mn–Ti oxides: Fe–Mg–Ti oxides and olivine, Am. Mineral. 76 (1991) 427–444.
[44] R.G. Berman, Internally-consistent thermodynamic data for minerals in the system Na_2O–K_2O–CaO–MgO–FeO–Fe_2O_3–Al_2O_3–SiO_2–TiO_2–H_2O–CO_2, J. Petrol. 29 (1988) 445–522.
[45] T.J.B. Holland, R. Powell, An enlarged and updated internally consistent thermodynamic dataset with uncertainties and correlations: the system K_2O–Na_2O–CaO–MgO–MnO–FeO–Fe_2O_3–Al_2O_3–TiO_2–SiO_2–C–H–O_2, J. Metamorph. Geol. 8 (1990) 89–124.

[46] R.A. Robie, B.S. Hemingway, Thermodynamic properties of minerals and related substances at 298.15 K and 1 bar (10^5 pascals) pressure and at higher temperature, U.S. Geol. Surv. Bull. 2131 (1995) 461 pp.
[47] J.A.D. Connolly, Multivariable phase diagrams: an algorithm based on generalized thermodynamics, Am. J. Sci. 290 (1990) 666–718.
[48] R.A. Robie, B.S. Hemingway, J.R. Fisher, Thermodynamic properties of minerals and related substances at 298.15 K and 1 bar (10^5 pascals) pressure and at higher temperatures, U.S. Geol. Surv. Bull. 1452 (1978) 456 pp.
[49] L. Wang, E.J. Essene, Y. Zhang, Mineral inclusions in pyrope crystals from Garnet Ridge, Arizona, USA: implications for processes in the upper mantle, Contrib. Mineral. Petrol. (1998) (in press).
[50] B.J. Wood, D. Virgo, Upper mantle oxidation state: ferric iron contents of lherzolite spinels by ^{57}Fe Moessbauer spectroscopy and resultant oxidation fugacities, Geochim. Cosmochim. Acta 53 (1989) 1277–1291.
[51] D. Canil, H.S.C. O'Neill, Distribution of ferric iron in some upper-mantle assemblages, J. Petrol. 37 (1996) 609–635.
[52] S. Foley, High-pressure stability of the fluor- and hydroxy-endmembers of pargasite and K-richterite, Geochim. Cosmochim. Acta 55 (1991) 2689–2694.
[53] R.O. Sack, M.S. Ghiorso, An internally consistent model for the thermodynamic properties of Fe–Mg–titanomagnetite–aluminate spinels, Contrib. Mineral. Petrol. 106 (1991) 474–505.
[54] B.A. Wyatt, P.J. Lawless, Ilmenite in polymict xenoliths from the Bultfontein and De Beers mines, South Africa, in: J. Kornprobst (Ed.), Kimberlites II: The Mantle and Crust–Mantle Relationships, Proc. 3rd Int. Kimb. Conf., Elsevier, Amsterdam, 1984, pp. 43–56.
[55] C.S. Kennedy, G.C. Kennedy, The equilibrium boundary between graphite and diamond, J. Geophys. Res. 81 (1976) 2467–2470.
[56] D.G. Pearson, F.R. Boyd, S.E. Haggerty, J.D. Pasteris, S.W. Field, P.H. Nixon, N.P. Pokhilenko, The characterisation and origin of graphite in cratonic lithospheric mantle: a petrological carbon isotope and Raman spectroscopic study, Contrib. Mineral. Petrol. 115 (1994) 449–466.
[57] V.K. Garanin, G.P. Kudryavtseva, A.D. Khar-kiv, V.F. Chistyakova, New eclogite variety in kimberlite pipes of Yakutia , Trans. (Dokl.) U.S.S.R. Acad. Sci. Earth Sci. Sect. 262 (1982) 147–151.
[58] F.R. Boyd, J.B. Dawson, J.V. Smith, Granny Smith diopside megacrysts from the kimberlites of the Kimberley area and Jagersfontein, South Africa, Geochim. Cosmochim. Acta 48 (1984) 381–384.
[59] G.P. Brey, T. Köhler, Geothermobarometry in four-phase lherzolites II, New thermobarometers, and practical assessment of existing thermobarometers, J. Petrol. 31 (1990) 1353–1378.
[60] D.H. Eggler, D.R. Baker, Reduced volatiles in the system C–O–H; implications to mantle melting, fluid formation, and diamond genesis, in: S. Akimoto, M.H. Manghnani (Eds.), High Pressure Research in Geophysics, Advances in Earth and Planetary Sciences (AEPS), Vol. 12, Center for Academic Publications Japan, Tokyo, 1982, pp. 237–250.
[61] K. Wei, R.W. Luth, Calibration of oxidation–reduction reaction at 1000–1400ºC and 5–9 GPa in the multianvil apparatus, EOS 74 (1993) 321.
[62] S.K. Saxena, N. Chatterjee, Y. Fei, G. Shen, Thermodynamic Data on Oxides and Silicates, Springer, Berlin, 1993, 428 pp.